RSC Advances

ROYAL SOCIETY OF CHEMISTRY

www.rsc.org/advances

Synthesis and Characterization of Hole-transporting Star-Shaped Carbazolyl Truxene Derivatives

Danusorn Raksasorn[1], Supawadee Namuangruk[2], Narid Prachumrak[3], Taweesak Sudyoadsuk[3], Vinich Promarak[3], Mongkol Sukwattanasinitt[1], Paitoon Rashatasakhon[1*]

[1]*Department of Chemistry, Faculty of Science, Chulalongkorn University, Bangkok 10330, Thailand*

[2]*National Nanotechnology Center, NSTDA, 111 Thailand Science Park, Klong Luang, Pathum Thani 12120, Thailand*

[3]*Department of Materials Science & Engineering, School of Molecular Science & Engineering, Vidyasirimedhi Institute of Science and Technology, Wongchan, Rayong 21210, Thailand*

E-mail: paitoon.r@chula.ac.th

Tel.: +66 (2) 2187633

Fax.: +66 (2) 2187598

Keywords

Truxene

Carbazole

Hole-transporting

C-N coupling

Organic Light-Emitting Diode

Electroluminescence

Abstract

Two star-shaped carbazolyl truxene derivatives (**1** and **2**) are synthesized via iodination of truxene and Cu-catalyzed C-N coupling with carbazole or 3,6-di(9-carbazolyl) carbazole. In solution phase, these compounds show maximum absorption bands around 330 nm and the emission maxima at 367 and 391 nm. The emission bands shift bathochromically in solid phase as a result of the more restricted molecular vibration and rotation. Both compounds show good thermal stabilities with glass transition temperatures at 249 and 293 ºC and 5% weight loss temperatures at 392 and 371 ºC, respectively. Both compounds exhibit good hole-transporting properties as the devices of structure ITO/PEDOT:PSS/**1** or **2** /Alq3/LiF:Al could provide maximum brightness of 12,000 cd/m^2 with turn-on voltages of 3.1-4.1 V, and maximum external quantum efficiency of 0.89-1.13%.

1. Introduction

Organic light-emitting diodes (OLEDs) have become an attractive display technology since the end of twentieth century due to their energy-saving nature and abilities to be fabricated as flat or flexible screens [1]. In a typical OLED device, there is a thin layer of emitting material (EM) sandwiched between cathode and anode. Upon electrical excitation, a recombination of electron from the LUMO and hole (positive charge) from the HOMO of the EM will result in the emission of visible light. As a result, much of the research in this field has been related to the development of emissive materials [2]. However, layers of hole-or electron-transporting material (HTM or ETM) can be fabricated between EM and electrodes in order to improve the device efficiency [3-4]. The most commonly used HTMs are *N,N'*-diphenyl-*N,N'*-bis(1-naphthyl)-(1,1'-biphenyl)-4,4'-diamine (NPB) and *N,N'*-bis(3-methylphenyl)-*N,N'*-bis(phenyl)benzidine (TPD), which have high hole mobility. However, low glass transition temperature (T_g) of NPB and TPD (100 and 65 °C, respectively) and poor morphological properties may lead to degradation of devices upon long-term uses. Most of the newly developed HTMs usually contain carbazole moieties due to their relatively small exchange energies associated with small orbital overlap in the n-π^* transition [5]. During our research program on design and synthesis of new optoelectronic materials, we became interested in truxene due to its unique emission property, high thermal stability, and ease of synthesis. It was regarded as a promising scaffold for future materials [6], which had been used in hole-transporting materials [7], blue fluorescent emitters [8], and many interesting C_3-symmetric materials [9].

There have been several examples of molecular designs which incorporate emissive and hole-transporting moieties into the same molecules [10]. These new optoelectronic materials not only offer superior properties, their applications would also reduce the fabrication steps on the electrodes. In this paper, we report an incorporation of this highly emissive polyaromatic truxene unit with carbazole fragments with an aim to achieve new OLED materials with hole-transporting properties. The structures of target compounds are shown in **Figure 1**.

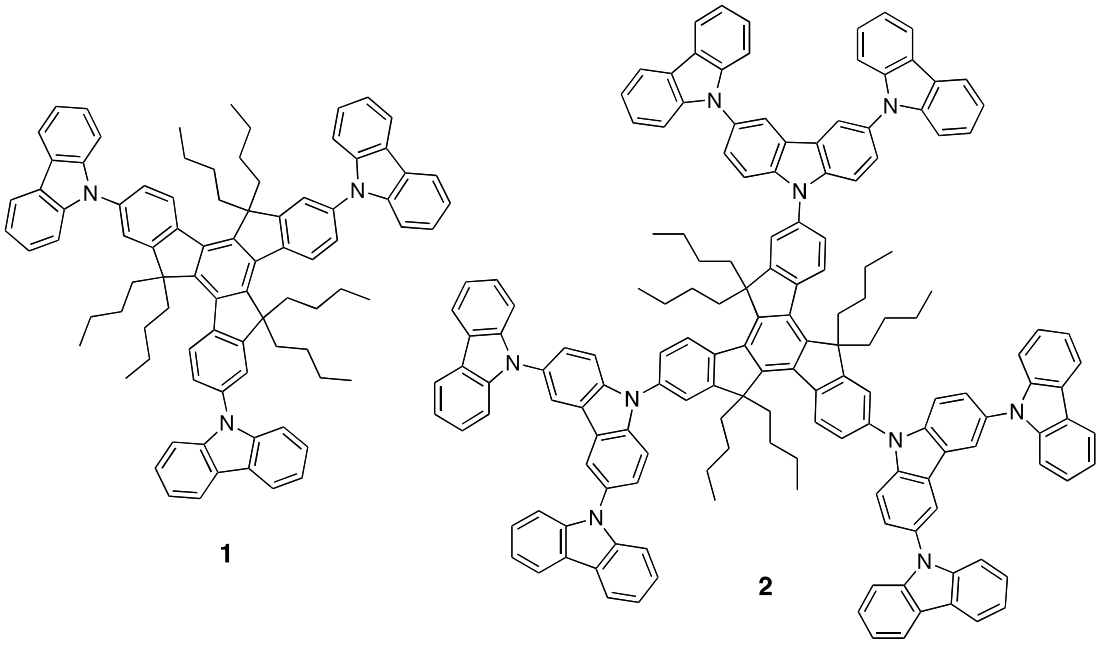

Figure 1. Structure of target **1** and **2**.

2. Experimental

2.1 Materials and instruments

All reagents were purchased from Aldrich, Fluka and used without further purification. All ^{1}H-NMR spectra were recorded on Varian Mercury 400 MHz NMR spectrometer (Varian, USA) using $CDCl_3$ and DMSO-d6. ^{13}C-NMR spectra were recorded at 100 MHz on Bruker NMR spectrometer using the same solvent. Mass spectra were recorded on a Microflex MALDI-TOF mass spectrometer (Bruker Daltonics) using doubly recrystallized α-cyano-4-hydroxy cinnamic acid (CCA) as a matrix. Elemental (CHN) analyses were performed on Perkin-Elmer 2400 series II (Perkin-Elmer, USA). Absorption spectra were measured by a Varian Cary 50 UV-Vis spectrophotometer. Fluorescence spectra were obtained from a Varian Cary Eclipse spectrofluorometer. Thermal experiments with Differential Scanning Calorimeter (DSC) were performed on Mettler Toledo DSC 822e and Thermogravimetric Analysis (TGA) was studied using Simultaneous Thermal Analyzer Netzsch 409. Cyclic voltammetry was performed using an AUTOLAB spectrometer with a glassy carbon working electrode, a platinum wire counter electrode, and a $Ag/AgNO_3$ reference electrode. All measurements were made at room temperature, scan rate 50 mV/s, on sample solutions in freshly distilled dichloromethane with 0.1 M tetrabutylammonium hexafluorophosphate as electrolyte and ferrocene/ferrocenium couple

as an internal standard. Dichloromethane was distilled from calcium hydride and the electrolyte solutions were degassed by nitrogen bubbling.

2.2 Synthesis procedures.

Truxene

This compound was synthesized according to the literature reports [11]. A mixture of 3-phenylpropionic acid (10.0 g, 66.7 mmol) and polyphosphoric acid (50 g) was heated at 60 °C for 60 min under nitrogen atmosphere. Water (5 mL) was then added to the reaction and temperature was raised to 160 °C for 3 h. After the reaction was cooled to room temperature, the mixture was poured into ice water and grey powder was filtered and washed with water. The crude product was purified by recrystallization from toluene to yield truxene as light-yellow solid (11.1 g, 49%). ^{1}H NMR ($CDCl_3$): δ 7.92 (d, J = 7.5 Hz, 1H), 7.68 (d, J = 7.3 Hz, 1H), 7.50 (t, J = 7.2 Hz, 1H), 7.39 (t, J = 7.2 Hz, 1H), 4.22 (s, 2H).

*5,5,10,10,15,15-Hexabutyl-truxene (**3**)*

A solution of truxene (1.0 g, 2.92 mmol) in DMF (50 mL) at 0 °C under nitrogen, NaH 60% (1.2 g, 29.8 mmol) was added and the solution was allowed to warm to room temperature and stirred for 30 min, then n-butyl bromide (3.2 mL) was added for 24 h. The mixture was poured into water and extracted with EtOAc. The combined organic layer was dried over $MgSO_4$, filtered, and concentrated under reduce pressure. The crude product was purified by silica gel column chromatography using hexane as the eluent to yield **3** as white solid (1.48 g, 75%). ^{1}H NMR ($CDCl_3$): δ 8.38 (d, J = 7.4 Hz, 1H), 7.47 (d, J = 5.9 Hz, 1H), 7.43 – 7.31 (m, 2H), 3.09 – 2.88 (m, 2H), 2.20 – 2.00 (m, 2H), 1.02 – 0.79 (m, 4H), 0.61 – 0.35 (m, 10H). This ^{1}H-NMR data agrees with the reference report. [12]

*5,5,10,10,15,15-Hexabutyl-2,7,12-triiodo-truxene (**4**)*

To a solution of **3** (0.50 g, 0.74 mmol) in 5 ml of solvent mixture (CH_3COOH : H_2SO_4 : H_2O = 100 : 40 : 3) was added 1 mL of CCl_4. After adding KIO_3 (0.16 g, 0.75 mmol) and I_2 (0.94 g, 3.72 mmol), the mixture was heated to 80 °C and stirred for 3 h. The reaction was cooled to room temperature and poured into water. The crude product was obtained by filtration and purified by recrystallization from ethanol to afford white powder (0.65 g, 84%). mp 312-314 °C. IR (KBr) ν_{max} cm^{-1}: 2953, 2915, 2849, 1453, 1353, 1180, 873, 823,

788. ^{1}H NMR ($CDCl_3$): δ 8.07 (d, J = 8.4 Hz, 1H), 7.76 (s, 1H), 7.71 (d, J = 8.4 Hz, 1H), 2.88 – 2.81 (m, 2H), 2.05 – 2.00 (m, 2H), 0.92 – 0.84 (m, 5H), 0.52 – 0.41 (m, 10H). This ^{1}H-NMR data agrees with the reference report. [12]

*Compound **1***

A mixture of **4** (0.11 g, 0.10 mmol), carbazole (0.12 g, 0.73 mmol), Cu bronze powder (0.17 g, 2.69 mmol) and K_2CO_3 (0.21 g, 1.53 mmol) in degassed nitrobenzene (1 mL) was refluxed for 48 h under N_2 atmosphere. The resulting brown solution was allowed to cool to room temperature, diluted with water (20 mL), and extracted with CH_2Cl_2 (3 × 50 mL). The combined organic layer was dried over $MgSO_4$, filtered, and concentrated under reduce pressure. The crude product was purified by silica gel column chromatography using 4:1 hexane/CH_2Cl_2 as the eluent to yield **1** (48.6 mg, 41%). ^{1}H NMR ($CDCl_3$): δ 8.60 (d, J = 8.5 Hz, 1H), 8.22 (d, J = 7.8 Hz, 2H), 7.73 (s, 1H), 7.66 (d, J = 8.3 Hz, 1H), 7.59 (d, J = 8.3 Hz, 2H), 7.49 (t, J = 7.2 Hz, 2H), 7.35 (t, J = 7.2 Hz, 2H), 3.15 – 3.02 (m, 2H), 2.27 – 2.15 (m, 2H), 1.13 – 1.01 (m, 4H), 0.79 – 0.75 (m, 4H), 0.62 (t, J = 7.3 Hz, 6H). ^{13}C NMR (100 MHz, $CDCl_3$): δ 155.5, 145.6, 140.9, 139.1, 138.1, 136.2, 125.95, 125.77, 124.7, 123.5, 120.8, 120.4, 120.0, 109.9, 56.0, 36.6, 26.7, 22.9, 13.9. MALDI-TOF-MS: found 1173.768 ($[M]^+$ calcd: 1173.690). Anal. Calcd for $C_{87}H_{87}N_3$: C, 88.96; H, 7.47; N, 3.58%; Found: C, 88.89; H, 7.56; N, 3.55%.

*Compound **2***

A mixture of **4** (0.11 g, 0.10 mmol), **5** (0.18 g, 0.37 mmol), Cu bronze powder (0.13 g, 2.05 mmol) and K_2CO_3 (0.22 g, 1.56 mmol) in degassed nitrobenzene (1 mL) was refluxed for 48 h under N_2 atmosphere. The resulting brown solution was allowed to cool to room temperature, diluted with water (20 mL), and extracted with CH_2Cl_2 (3 × 50 mL). The combined organic layer was dried over $MgSO_4$, filtered, and concentrated under reduce pressure. The crude product was purified by silica gel column chromatography using 4:1 hexane/CH_2Cl_2 as the eluent to yield **2** (0.11 g, 50%). ^{1}H NMR ($CDCl_3$): δ 8.80 (d, J = 8.5 Hz, 1H), 8.40 (s, 2H), 8.22 (d, J = 7.5 Hz, 4H), 7.99 (s, 1H), 7.96 – 7.85 (m, 3H), 7.75 (d, J = 8.7 Hz, 2H), 7.55 – 7.40 (m, 8H), 7.34 (t, J = 7.1 Hz, 4H), 3.33 – 3.20 (m, 2H), 2.48 – 2.36 (m, 2H), 1.27 – 1.10 (m, 4H), 1.03 – 0.80 (m, 4H), 0.72 (t, J = 7.3 Hz, 6H). ^{13}C NMR (100 MHz, $CDCl_3$): δ 156.2, 146.2, 142.0, 140.9, 139.9, 138.4, 136.0, 130.8, 126.6, 126.3, 126.1, 125.2, 124.4, 123.4, 121.2, 120.5, 120.1, 119.9, 111.5, 109.9, 56.5, 37.0, 27.0, 23.1,

14.2. MALDI-TOF-MS: found 2165.802 ($[M]^+$ calcd: 2164.037). Anal. Calcd for $C_{159}H_{129}N_9$: C, 88.18; H, 6.00; N, 5.82%; Found: C, 88.25; H, 6.06; N, 5.69%.

2.3. OLED fabrication and measurement

Three double layer devices (I-III) were fabricated with **1** and **2** as HTL and Alq_3 as the electron-transporting layer (ETL) and emitting layer. The patterned indium tin oxide (ITO) glass substrate with a sheet resistance 14 Ω/sq (purchased from Kintec Company) was thoroughly cleaned by successive ultrasonic treatment in detergent, deionised water, and acetone, and then dried at 100 ^oC in a vacuum oven. A 50 nm thick PEDOT:PSS hole injection layer was spin-coated on top of ITO from a 0.75 wt.% dispersion in water at a spin speed of 2500 rpm for 30 s and dried at 100 ^oC for 15 min under vacuum. Thin films of HTL were deposited on top of PEDOT:PSS layer by spin-coating THF : toluene solution of compound **1** and **2** (2% w/v) on an ITO glass substrate at a spin speed of 2500 rpm for 30 second. Then Alq_3 was deposited onto the surface of the HTL film as light-emitting (EML) and electron-transporting layer (ETL) with a thickness of 50 nm by evaporation from resistively heated alumina crucibles at evaporation rate of 0.5-1.0 nm/s in vacuum evaporator deposition (ES280, ANS Technology) under a base pressure of ~10^{-5} mbar. The film thickness was monitored and recorded by quartz oscillator thickness meter (TM-350, MAXTEK). The chamber was vented with dry air to load the cathode materials and pumped back; a 0.5 nm thick LiF and a 150 nm thick aluminium layers were the subsequently deposited through a shadow mask on the top of EML film without braking vacuum to from an active diode areas of 4 mm^2. The measurement of device efficiency was performed according to M.E. Thomson's protocol and the device external quantum efficiencies were calculated using procedure reported previously. Current density-voltage-luminescence (J-V-L) characteristics were measured simultaneous by the use of a Keithley 2400 source meter and a Newport 1835C power meter equipped with a Newport 818-UV/CM calibrated silicon photodiode. The EL spectra were acquired by an Ocean Optics USB4000 multichannel spectrometer. All the measurements were performed under ambient atmosphere at room temperature.

3. Results and discussion

*3.1 Synthesis of **1** and **2***

The synthesis procedures are outlined in **Scheme 1**. Upon the preparation of truxene from 3-phenylpropionic acid according to the reported procedure [11], the methylene units were

alkylated by excess amount of *n*-butylbromide to afford **3** in 75%. This hexaalkylated compound exhibit greater solubility in organic solvents, which facilitate not only the purification process of the target and intermediate molecules, but also prevention of the aggregation by pi-stacking which could lead to low quantum efficiencies. Treatment of **3** with KIO_3 and I_2 produced triiodo **4** which reacted with carbazole in the presence of catalytic amount of Cu bronze to afford **1** in moderate yield of 34% for 2 steps. The target compound **2** was also synthesized in 50% yield by the Cu-catalyzed C-N coupling of **4** with 3,6-di(9-carbazolyl) carbazole (**5**) which was prepared according to a literature procedure [13].

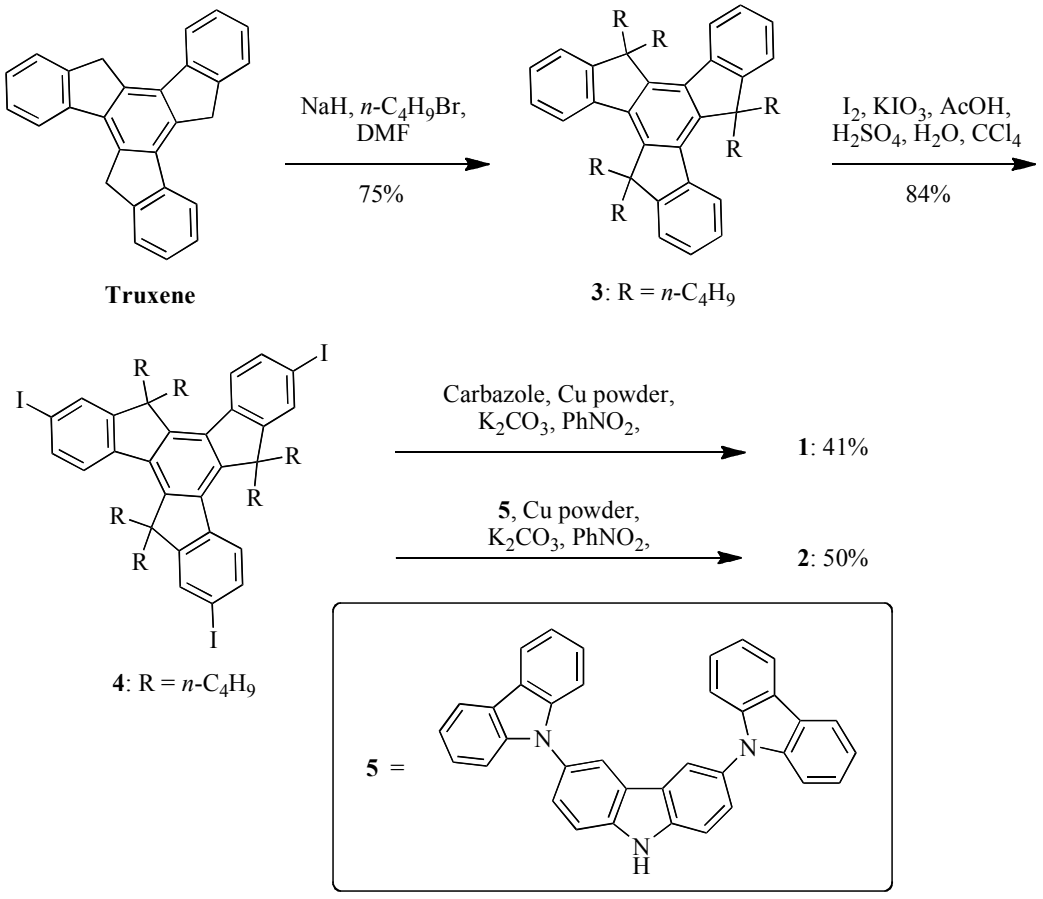

Scheme 1 Synthesis of **1** and **2**

*3.2 Photophysical properties of **1** and **2***

Table 1 summarizes the photophysical properties of **1** and **2** in diluted chloroform solution and in thin film. In solution phase, both compounds showed two strong absorption bands at

294 and 330 nm corresponding to the π-π* electron transition for the carbazole and truxene pendants, respectively (**Figure 2**). The similarity in their absorption spectra suggested that the π-conjugation systems in **1** and **2** were quite similar, and the steric hindrance caused by the outer carbazole groups in **2** may prevent full conjugation throughout the entire molecule. The absorption bands of **1** and **2** in solid state appeared at 315 and 333 nm, respectively (**Figure 3**). The bathochromic shifting of the absorption band in **2** may cause by a more effective conjugation induced by the solid-state packing. With a higher number of photoactive carbazole units, the molar absorptivity of **2** was slightly higher than that of **1**. The onset absorptions for **1** and **2** appeared at 420 nm and 402 nm, corresponding to energy band gaps of 2.95 eV and 3.08 eV, respectively.

In solution phase, the emission spectra of these compounds displayed a typical vibrational progression pattern of truxene core with maximum emission wavelengths at 367 and 391 nm for **1** and **2**, respectively (**Figure 2**). The longer emission maxima for **2** indicated a higher degree of geometrical relaxation upon excitation cause by the more carbazole units. This might also cause a lower quantum efficiency of **2** (0.10) as compared to that of **1** (0.22). In the solid state, the emission maxima of **1** and **2** bathochromically shifted to 379 and 418 nm, respectively (**Figure 3**).

Table 1 Photophysical and electrochemical properties of **1** and **2**

Cpd.	$\boldsymbol{\lambda_{max}^{abs}}$[nm] (log ε [$M^{-1}cm^{-1}$])		$\boldsymbol{\lambda_{max}^{emit}}$[nm]		Φ_F [a]	E_g [b] [eV]	HOMO [c] [eV]	LUMO [d] [eV]
	Solution	Solid	Solution	Solid				
1	331 (4.95)	315	367	379	0.22	2.95	-5.19	-2.24
2	330 (5.05)	333	391	418	0.10	3.08	-5.07	-1.99

[a] 2-aminopyridine in 0.1 M H_2SO_4 (Φ_F = 0.60) was the reference. [b] The optical energy gap estimated from the onset of the absorption spectra ($E_g = 1240/\lambda_{onset}$). [c] Measured using a glassy carbon as a working electrode, a platinum wire as a counter electrode, and $Ag/AgNO_3$ as a reference electrode in CH_2Cl_2 containing 0.1M $TBAPF_6$ as a supporting electrolyte at a scan rate of 50 mV/s under a nitrogen atmosphere. Calculated by the empirical equation: $HOMO = -(E_{onset}-E_{Fc/Fc+}+4.8)$. [d] Calculated from LUMO = HOMO - E_g.

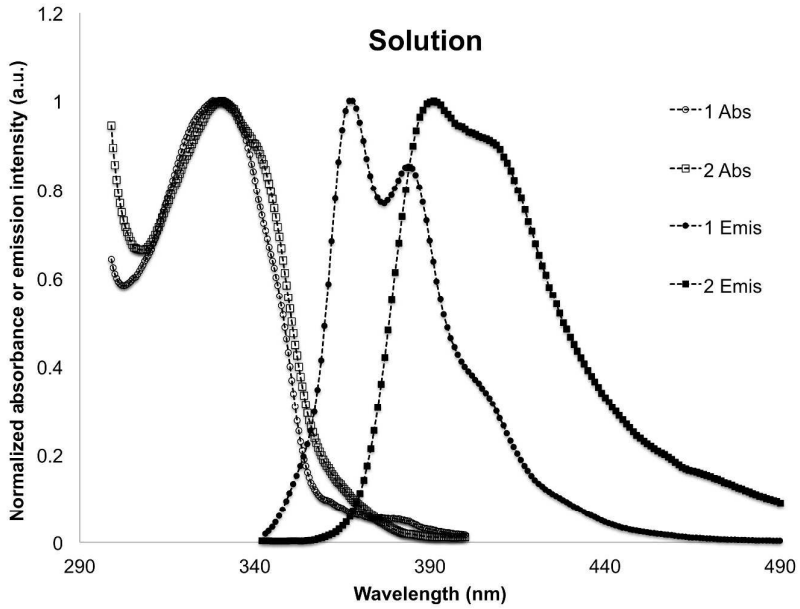

Figure 2 Absorption and emission spectra of **1** and **2** in $CHCl_3$ solution.

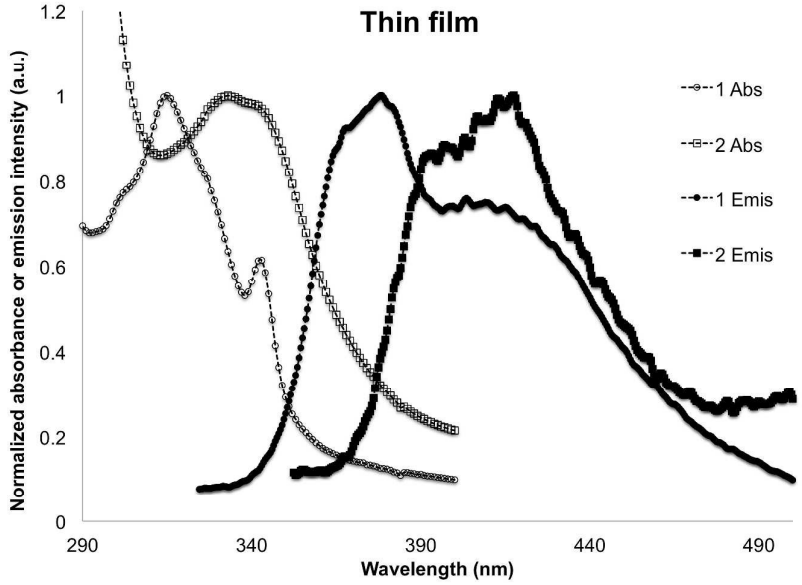

Figure 3 Absorption and emission spectra of **1** and **2** in thin film state.

3.3 Thermal properties

The thermal properties of **1** and **2** were investigated by differential scanning calorimetry (DSC) and thermogravimetric analysis (TGA). The TGA data suggested that all compounds were thermally stable with 5% weight loss temperature ($T_d^{5\%}$) at 392 and 371

^{o}C, respectively. From the second heating cycle on DSC (**Figure 4**), compound **1** showed only an endothermic peak at 249 ^{o}C due to glass transition temperature (T_g) and no signal for melting and crystallization temperature was observed. For compound **2**, the higher glass transition temperature (T_g) at 293 ^{o}C was observed, which indicate that the higher numbers of carbazole units may lead to a lower degree of molecular rotation and vibration. These results suggested these new compounds could form molecular glass with T_g higher than those of the commercially available and commonly used HTMs.

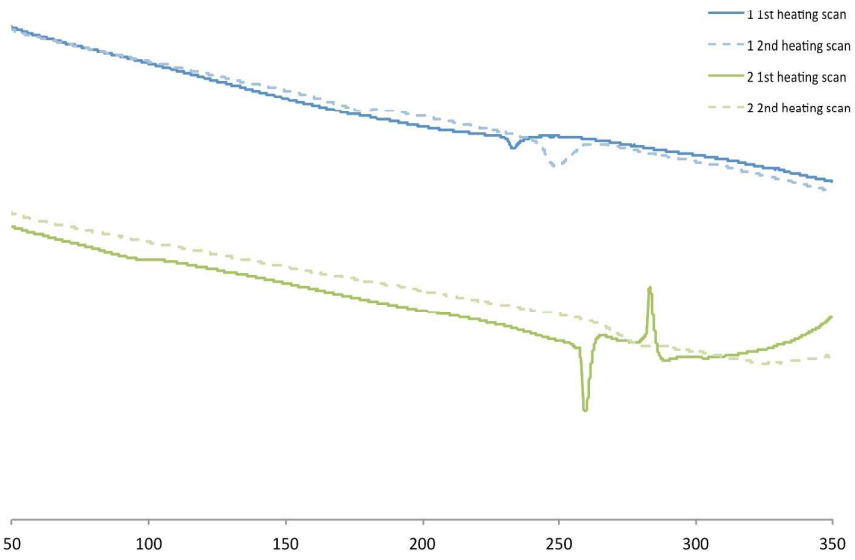

Figure 4 DSC curves of **1** and **2** at a heating rate of 10 ^{o}C/min under N_2 atmosphere

3.4 Electrochemical properties

The electrochemical properties of **1** and **2** were investigated by cyclic and differential pulse voltammetric techniques. The results were summarized in **Table 1** and **Figure 5**. The HOMO energy level of compound **1** and **2** were estimated as -5.19 and -5.07 eV, respectively, from an empirical formula, HOMO = -(E_{onset}-$E_{Fc/Fc+}$+4.8) (eV) [14]. The lower oxidation of **2** referred to the longer π-conjugation. The LUMO energy level were calculated by HOMO energy level subtracted with energy gap from absorption spectra, to

be -2.24 and -1.99 eV. These suggested that **2** could be oxidized easier and may have better hole-transporting property than **1**.

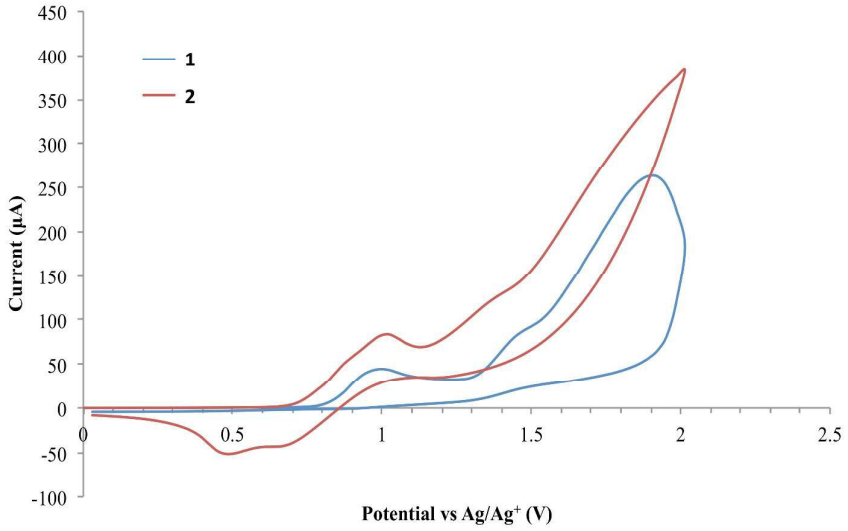

Figure 5 Cyclic voltamograms of **1** and **2.**

3.5 Quantum chemical calculation

To further understand the electronic properties and geometries of these two compounds, their structures were optimized by B3LYP/6-31G(d,p) method. All computations were performed by GAUSSIAN 09 [15]. The results revealed that the substituted carbazole moieties were twisted to the core of the compounds. The average dihedral angle of the first shell carbozole moieties of **1** is about 54 degrees, while that of **2** is relative larger for about 2 degrees (**Figure 6**). It is noted that the dihedral angle of the second shell carbozole moieties is about 60 degrees. These twisting should affect the electronic communication among these fragments and the overall photophysical properties of the compounds. In compound **1**, HOMO shows that electron density is delocalized over the whole molecule, while the electron density of the LUMO is in the core (**Figure 7**). This indicates that electron can delocalized over the entire molecule if it is irradiated by light. The HOMO of **2** is quite different from that of **1** in which only one of the three braches is occupied by electron density. These may be affected by large dihedral angle of the second shell of substituted carbazoles. The calculated energy difference between HOMO and LUMO (Δ_{H-L}) of the two compounds are 3.93 and 3.48 eV for **1** and **2**, respectively. The lower Δ_{H-L} of **2** is due to its low LUMO energy which is stabilized by high degree substituted carbazoles.

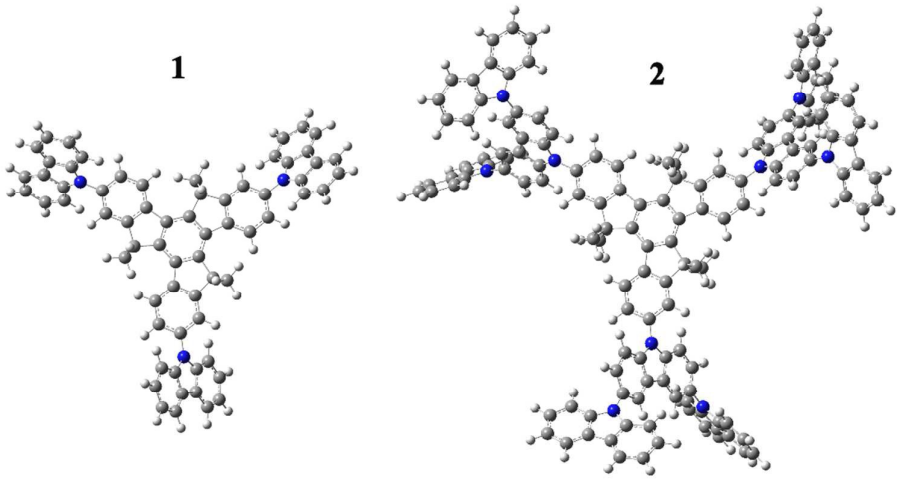

Figure 6. Optimized structure of **1** and **2**.

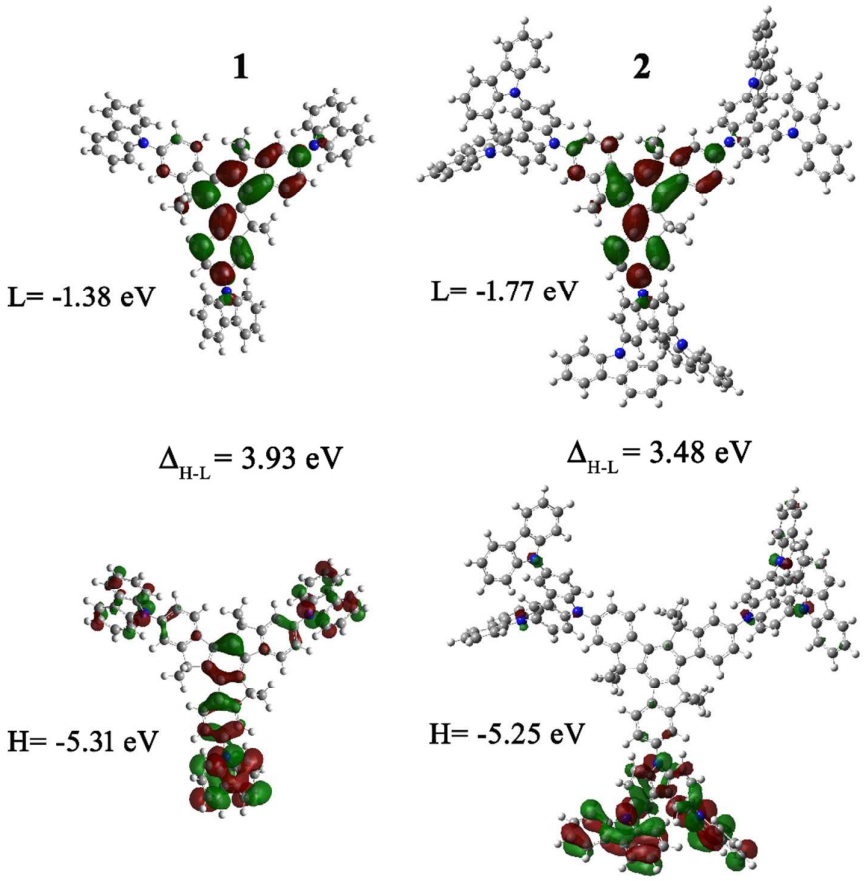

Figure 7. Calculated HOMO (H), LUMO (L), and HOMO-LUMO gap (Δ_{H-L}) of **1** and **2**.

3.6 Hole transporting properties

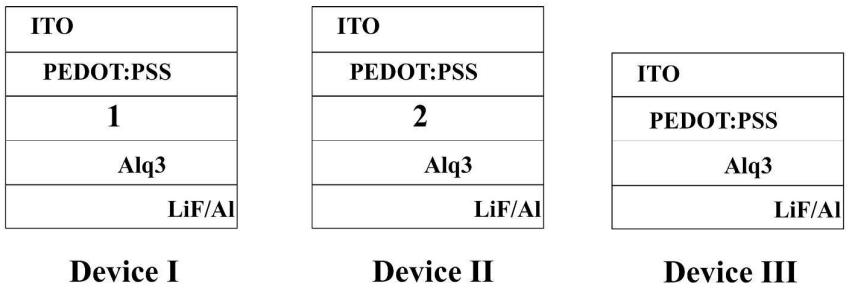

Figure 8. Configuration of **Device I-III**.

From the electronic properties of **1** and **2**, it was found that the HOMO-LUMO levels of **1** and **2** are suitable for the work functions of the ITO and LiF/Al electrodes and Alq_3 green emissive material. To investigate the hole transporting properties of these compounds, two multi-layer OLED devices were fabricated using **1** and **2** as hole-transporting layer (Device I-II, **Figure 8**). The reference device (III) fabricated without a HTL was made. The comparison of device efficiencies to those of Device III would then suggest the performances of **1** and **2**. The detailed EL and J–V–L data are shown in **Figure 9** and summarized in Table 2. Comparison with Device III reveals that the incorporation of **1** and **2** as HTL in the Device I, II not only increases the maximum luminance (L_{max}) and luminance efficiency (η), but also decreases the V_{on} of the diodes, signifying the hole-transporting ability of both compounds. The **1**-based green OLED (Device I) displays the best device performance with a high maximum brightness of 12,453 cd/m^2 at 11.2 V, a η_{max} of 4.60 cd/A at current density of 13.5 mA/cm^2 and a maximum external quantum efficiency (EQE) of 1.13%. Under applied voltages, the devices (I, II) emit a bright green emission with peak centred at 522-521 nm and CIE coordinates of (0.29, 0.53), which suggested that **1** and **2** only functioned as the hole transporting materials. The EL spectra (**Figure 9a**) are matched with the PL spectrum of Alq3, the EL of the reference device (III) and also other reported EL spectra of Alq3-based devices [16]. No emission at the longer wavelength owing to exciplex species formed at the interface of HTL and EML materials, which often occurs in the devices fabricated from HTL with planar molecular structure, is observed [17]. From these results and in view of the fact that a barrier for electron migration at the Alq3/HTL interface (0.76-1.01 eV) is larger than those for hole migration at the HTL/Alq3 interface (0.61–0.73 eV). Hence, under the present device structure, **1** and

2 act only as HTL, and Alq3 acts preferably as an electron blocker more than as a hole blocker and charge recombination thus limited to Alq3 layer.

Table 2 Electroluminescent performances of Device I-III**.**

Device	HTL[a]	λ^{EL}_{max}/FWHM (nm)	V_{on}/V_{100} (V)[b]	L_{max} at voltage (cd m^{-2}/V)[b]	J_{max} (mA cm^{-2})[d]	η_{max}/η at L_{100}/η at L_{1000} (cd A^{-1})[e]	EQE (%)[f]	CIE (x,y)
I	**1**	522 (95)	4.1/5.7	12453 (11.2)	610	4.60 (13.5)/4.50/4.47	1.13	0.29, 0.53
II	**2**	521 (84)	3.1/4.4	12406 (10.2)	648	3.61 (51.5)/3.11/3.54	0.89	0.30, 0.54
III	none	518 (90)	4.2/5.4	4961 (10.0)	693	0.91 (366.8)/0.73/0.82	0.15	0.30, 0.54

[a] ITO/PEDOT:PSS/**HTL**/Alq3/LiF:Al. [b] Turn-on voltages at 1 and 100 cd m^{-2}. [c] Maximum luminance at applied voltage. [d] Current density. [e] Luminance efficiencies at maximum, at luminance of 100 and 1000 cd m^{-2}. [f] Maximum external quantum efficiency.

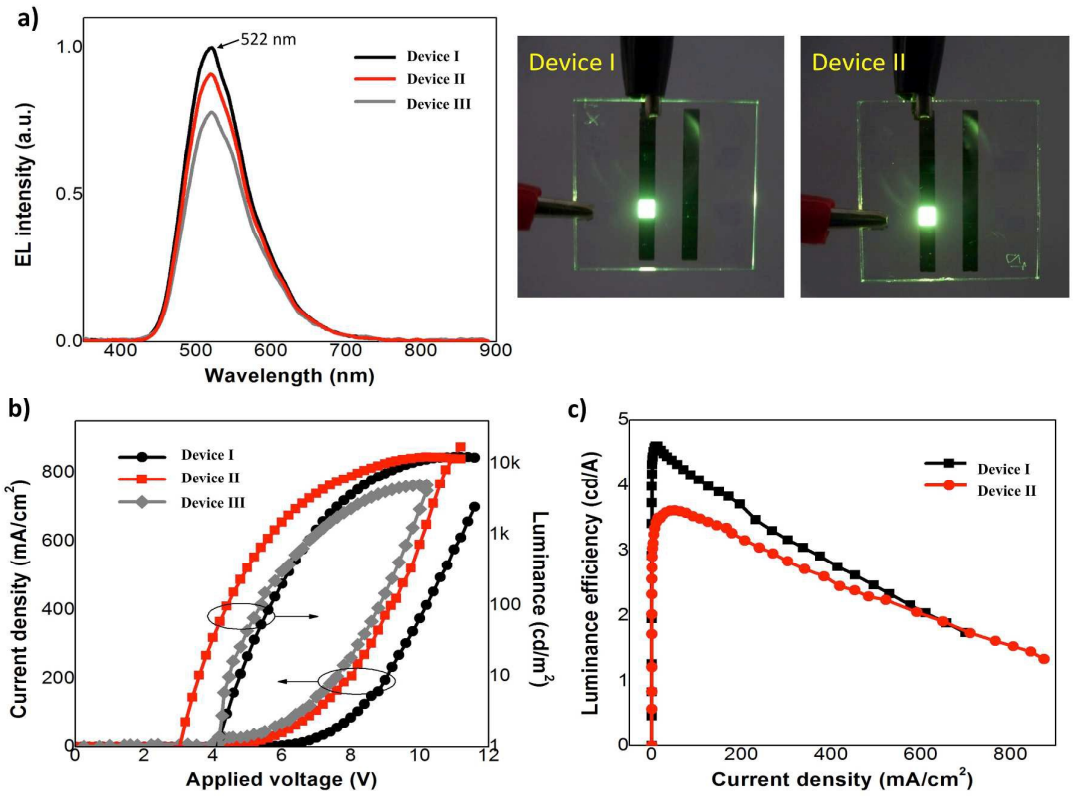

Figure 9 a) Electroluminescence spectra of Device I-III and photographic images of working Device I-II; **b)** J-V-L plots for Device I-III; **c)** Luminance efficiency-Current density plots.

4. Conclusions

Two derivatives of carbazole and truxene were successful synthesized by iodination of truxene core and Cu-catalysed C-N coupling with carbazole or 3,6-di-(9-carbazolyl) carbazole. With six n-butyl groups substituted on the truxene core preventing aggregation by π-stacking, the compounds were well soluble in organic solvents and can be casted into this solid film by spin-casting technique. In addition, both compounds were thermally stable and could form molecular glass with high T_g. Both compounds served as good hole-transporting materials for OLED devices with Alq3 emissive layer to afford maximum brightness of 12,000 cd/m^2 with turn-on voltages of 3.1-4.1 volt, and maximum external quantum efficiency of 0.89-1.13%.

Acknowledgements

This research has been supported by the Ratchadaphiseksomphot Endowment Fund (2013) of Chulalongkorn University (CU-56-425-AM).

References

[1] (a) N.T. Kalyani, S.J. Dhoble, Renew. Sust. Energ. Rev. 16 (2012) 2696; (b) F. Hide, M.A. Diaz-Garcia, B.J. Schartz, A.J. Heeger, Accounts Chem. Res. 30 (1997) 430; (c) J.H. Burroughes, D.D.C. Bradley, A.R. Brown, R.N. Marks, K. Mackey, R.H. Frien, P.L. Burns, A.B. Holmes, Nature 347 (1990) 539.

[2] (a) T.M. Figueira-Duarte, K. Mullen, Chem. Rev. 111 (2011) 7260; (b) S.-C. Lo, P.L. Burn, Chem. Rev. 107 (2007) 1097; (c) J. Kido, Y. Okamoto, Chem. Rev. 102 (2002) 2357.

[3] (a) C.-Y. Hsu, Y.-C. Chen, T. Y.-Y. Lin, K.-C. Ho, J.T. Lin, Phys Chem Chem Phys 14 (2012) 14099; (b) A. Iwan, D. Sek, Prog. Polym. Sci. 36 (2011) 1277; (c) Q. Huang, G.A. Evmenenko, P. Dutta, P. Lee, N.R. Armstrong, T.J. Marks, J. Am. Chem. Soc. 127 (2005) 10227.

[4] (a) J. Shen, D. Wang, E. Langlois, W.A. Barrow, P.J. Green, C.W. Tang, J. Shi, Synth. Met. 111-112 (2000) 233; (b) D.Y. Kondakov, J.R. Sandifer, C.W. Tang, R.H. Young, J. Appl. Phys. 93 (2003) 1108; (c) A.P. Kulkarni, C.J. Tonzola, A. Babel, S.A. Jenekhe, Chem. Mater. 16 (2004) 4556.

[5] (a) J.-H. Pan, H.-L. Chiu, B.-C. Wang, J. Mol. Struct. THEOCHEM. 725 (2005) 89; (b) N. Seidler, S. Reineke, K. Walzer, B. Lüssem, A. Tomkeviciene, J.V.

Grazulevicius, K. Leo, Appl. Phys. Letts 96 (2010) 093304. (c) A. Tomkeviciene, J.V. Grazulevicius, K. Kazlauskas, A. Gruodis, S. Jursenas, T.-H. Ke, C.-C. Wu, J. Phys. Chem. C. 115 (2011) 4887;

[6] F. Goubard, F. Dumur, RSC Adv. 5 (2015) 3521.

[7] Z. Yang, B. Xu, J. He, L. Xue, Q. Guo, H. Xia, W. Tian. Org. Electron. 10 (2009) 954.

[8] C. Yao, Y. Yu, X. Yang, H. Zhang, Z. Huang, X. Xu, G. Zhou, L. Yue, Z. Wu. J. Mater. Chem. C. 3 (2015) 5783.

[9] (a) L.-L. Li, P. Hu, B.-Q. Wang, W.-H. Yu, Y. Shimizu , K.-Q. Zhao, Liq. Cryst. 37 (2010) 499; (b) R. Misra, R. Sharma, S.M. Mobin, Dalton Trans. 43 (2014) 6891.

[10] (a) T. Kumchoo, V. Promarak, T. Sudyoadsuk, M. Sukwattanasinitt, P. Rashatasakhon, Chem.-Asian J. 5 (2010) 2162; (b) P. Moonsin, N. Prachumrak, S. Namuangruk, S. Jungsuttiwong, T. Keawin, T. Sudyoadsuk, V. Promarak, Chem. Commun. 49 (2013) 6388; (c) T. Khanasa, N. Prachumrak, R. Rattanawan, S. Jungsuttiwong, T. Keawin, T. Sudyoadsuk, T. Tuntulani, V. Promarak, Chem. Commun. 49 (2013) 3401.

[11] (a) M.S. Yuan, Q. Fang, Z.Q. Liu, J.P. Guo, H.Y. Chen, W.T. Yu, G. Xue, D.S. Liu. J. Org. Chem. 71 (2006) 7858; (b) N. Earmrattana, M. Sukwattanasinitt, P. Rashatasakhon, Dyes Pigments. 93 (2012) 1428.

[12] P. Sam-ang, D. Raksasorn, M. Sukwattanasinitt, P. Rashatasakhon, RSC Adv. 4 (2014) 58077.

[13] V. Promarak, M. Ichikawa, T. Sudyoadsuk, S. Saengsuwan, S. Jungsuttiwong, T. Keawin, Thin Solid Films. 516 (2008) 2881.

[14] (a) R. Cervini, X.-C. Li, G.W.C. Spencer, A.B. Holmes, S.C. Moratti, R.H. Friend, Synth. Met. 84 (1997) 359, (b) B.W. D'Andrade, S. Datta, S.R. Forrest, P. Djurovich, E. Polikarpov, M.E. Thompson, Org. Electron 6 (2005) 11.

[15] M. J. Frisch, G. W. Trucks, H. B. Schlegel, G. E. Scuseria, M. A. Robb, J. R. Cheeseman, G. Scalmani, V. Barone, B. Mennucci, G. A. Petersson, H. Nakatsuji, M. Caricato, X. Li, H. P. Hratchian, A. F. Izmaylov, J. Bloino, G. Zheng, J. L. Sonnenberg, M. Hada, M. Ehara, K. Toyota, R. Fukuda, J. Hasegawa, M. Ishida, T. Nakajima, Y. Honda, O. Kitao, H. Nakai, T. Vreven, J. A. Montgomery, J. E. Peralta, F. Ogliaro, M. Bearpark, J. J. Heyd, E. Brothers, K. N. Kudin, V. N. Staroverov, R. Kobayashi, J. Normand, K. Raghavachari, A. Rendell, J. C. Burant, S. S. Iyengar, J. Tomasi, M. Cossi, N. Rega, J. M. Millam, M. Klene, J. E. Knox, J. B. Cross, V. Bakken, C. Adamo, J. Jaramillo, R. Gomperts, R. E. Stratmann, O. Yazyev, A. J.

Austin, R. Cammi, C. Pomelli, J. W. Ochterski, R. L. Martin, K. Morokuma, V. G. Zakrzewski, G. A. Voth, P. Salvador, J. J. Dannenberg, S. Dapprich, A. D. Daniels, Farkas, J. B. Foresman, J. V. Ortiz, J. Cioslowski and D. J. Fox, Wallingford CT, 2009.

[16] (a) Y.K. Kim, S.-H. Hwang, Synth. Met., 156 (2006) 1028-1035; T. Keawin, C. Sooksai, N. Prachumrak, T. Kaewpuang, D. Muenmart, S. Namuangruk, S. Jungsuttiwong, T. Sudyoadsuk, V. Promarak, RSC Adv., 5 (2015) 16422–16432. (b) A.M. Thangthong, D. Meunmart, N. Prachumrak, S. Jungsuttiwong, T. Keawin, T. Sudyoadsuk, V. Promarak, Chem. Commun., 47 (2011) 7122-7124.

[17] U. Mitschke, P. Ba`Euerle, J. Mater. Chem., 10 (2000) 1471-1507.